SCIENTIFIC REPORTS

OPEN

Role of Ag_2S coupling on enhancing the visible-light-induced catalytic property of TiO_2 nanorod arrays

Received: 09 October 2015
Accepted: 17 December 2015
Published: 21 January 2016

Zhengcao Li[1,2], Shan Xiong[1], Guojing Wang[1], Zheng Xie[1,3] & Zhengjun Zhang[2]

In order to obtain a better photocatalytic performance under visible light, Ag_2S-coupled TiO_2 nanorod arrays (NRAs) were prepared through the electron beam deposition with glancing angle deposition (GLAD) technique, annealing in air, followed by the successive ionic layer absorption and reaction (SILAR) method. The properties of the photoelectrochemical and photocatalytic degradation of methyl orange (MO) were thus conducted. The presence of Ag_2S on TiO_2 NRAs was observed to have a significant improvement on the response to visible light. It's resulted from that Ag_2S coupling can improve the short circuit photocurrent density and enhance the photocatalytic activity remarkably.

Recently, as the demands of industrial wastewater treatment and solar energy conversion increasing, photocatalytic technology has become one of the most popular subjects. Since the photocatalytic splitting of water by titanium dioxide (TiO_2) electrodes was discovered by Fujishima *et al.* in 1972[1], TiO_2-based photocatalysis[2–8] has been extensively investigated due to its outstanding properties such as strong photocatalytic activity, chemical inertness, nontoxicity and low cost. However, there are still a couple of remained problems in utilizing TiO_2 as photocatalytic material. One is the light absorption limitation in visible light region due to the wide band-gap of TiO_2 (3.2 eV as anatase and 3.0 eV as rutile), the other is the easy recombination of photo-electrons and holes during the photocatalytic process. Hence, some recent studies have been carried out focusing on TiO_2 response in visible light region by different methods, which include sensitization with dyes[9,10], doping TiO_2 with metal or non-metal ions[11–13], and coupling TiO_2 with narrow band-gap semiconductors[14–18].

Among these methods, coupling TiO_2 with narrow band-gap semiconductors to form heterojunction structures shows promising effects in enhancing separation of photogenerated charge carriers and improving catalytic activity of TiO_2[19]. Compared with bare TiO_2, CdS-coupled TiO_2 presents a significant improvement on photocatalytic degradation of organic pollutants in industrial wastewater under visible light irradiation[20]. Nevertheless, the potential of releasing threatening Cd element is one major limitation for the application of this photocatalytic system[21]. Therefore, some other materials[22–26] (such as PbS, Ag_2S, WO_3, ZnO, SnO_2, α-Fe_2O_3 and so forth) have been investigated, and the non-toxic Ag_2S has a narrow energy gap of $E_g \sim 1.0$ eV, showing promising coupling performance with TiO_2. This is because that Ag_2S can facilitate charge carrier separation at the heterojunction interface[27], and increase the system's photocatalytic efficiency. In addition, low-dimensional nanostructures of TiO_2 coupled with nanoparticle sensitizers are expected to exhibit desirable photocatalytic activity by facilitating the charge carriers' transfer and reducing recombination centers[28]. In previous reports, there have been some positive results of Ag_2S-coupled TiO_2 nanotubes[29] and nanorods[30,31] in photovoltaic devices and water splitting areas. However, as far as we know, there are few work on the relation between the degradation efficiency and the amount of Ag_2S on the surface of TiO_2.

Herein, we successfully synthesized the visible-light-induced TiO_2 nanorods arrays (NRAs) coupled with different amounts of Ag_2S nanoparticles (NPs) by using the successive ionic layer absorbance and reaction (SILAR) method. The TiO_2 NRAs were obtained by oxidation of Ti NRAs, which were fabricated by electron beam deposition. The optimal as-prepared ultra-thin films with thickness of ~160 nm have shown pronounced short circuit photocurrent density improvement and remarkable photocatalytic activity enhancement compared with bare TiO_2 NRAs under visible light.

[1]State Key Laboratory for New Ceramics and Fine Processing, School of Materials Science and Engineering, Tsinghua University, Beijing 100084, China. [2]Key Laboratory of Advanced Materials (MOE), School of Materials Science and Engineering, Tsinghua University, Beijing 100084, China. [3]High-Tech Institute of Xi'an, Shanxi 710025, China. Correspondence and requests for materials should be addressed to Z.L. (email: zcli@mail.tsinghua.edu.cn)

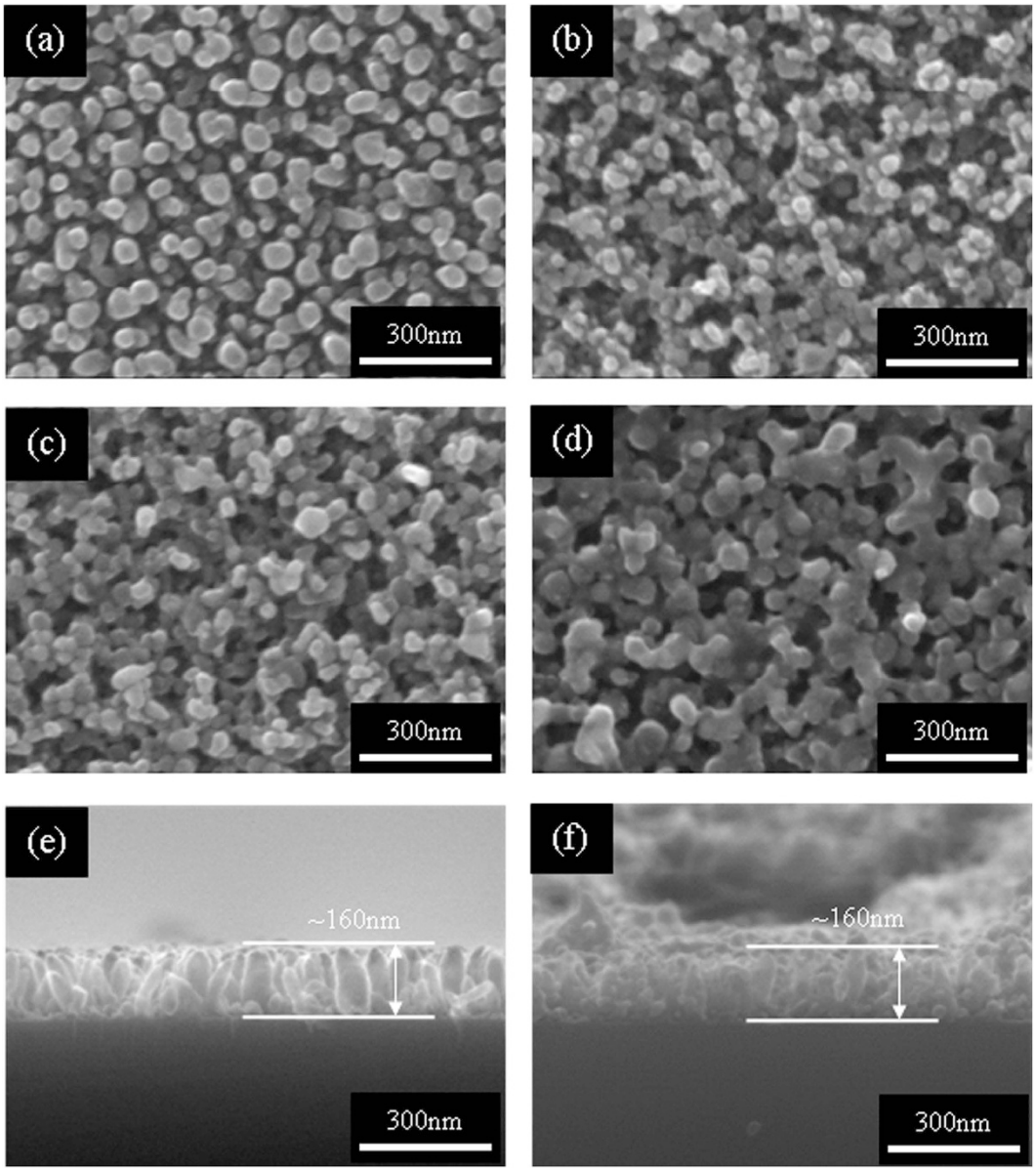

Figure 1. Top view SEM images of (**a**) bare TiO_2, and different Ag_2S-coupled TiO_2 NRAs by SILAR method for (**b**) 20 cycles, (**c**) 30cycles, (**d**) 40 cycles; and side view of (**e**) bare TiO_2 and (**f**) Ag_2S-coupled TiO_2 NRAs for 20 cycles.

Results

Characterization of Ag_2S-coupled TiO_2 NRAs. Figure 1a shows the typical top view SEM images of the bare TiO_2 film (before SILAR, 0 cycle). It can be clearly seen that TiO_2 film consists of separate nanorods with an average diameter of 50 nm. After depositing Ag_2S for 20, 30 and 40 cycles, the typical top view SEM images are shown in Fig. 1b–d, respectively. Without destructing the ordered TiO_2 NRAs structure, Ag_2S NPs were successfully deposited on the surface of TiO_2 NRAs with different diameters from 20 to 40 cycles and the deposition amount can be readily controlled by SILAR cycles. The side view of bare TiO_2 shows uniform NRAs with an average length of ~160 nm, as shown in Fig. 1e. As a representative example, the side view SEM image of 20-cycle sample is also given in Fig. 1f, which shows the length of the fabricated Ag_2S-coupled TiO_2 NRAs are ~160 nm as well.

Further observation of Ag_2S-coupled TiO_2 NRAs (35-cycle sample) has been confirmed by the high resolution transmission electron microscope (HRTEM) (shown in Fig. 2). The observed lattice distance of 0.316 nm and 0.246 nm corresponded to the (110) atomic planes of rutile TiO_2 and (112) atomic planes of Ag_2S, respectively. The HRTEM image also confirms Ag_2S nanocrystallines (with a diameter of 5 to 20 nm) coating on TiO_2 NRAs, as shown in Fig. 2.

Figure 3 displays the UV-visible absorption spectra of the Ag_2S-coupled TiO_2 NRAs with different SILAR cycles (n), from 0 to 40 cycles, respectively. For bare TiO_2 NRAs (0 cycle), there is a clear absorption enhancement in the wavelength of 390 nm, corresponding to the bandgap of anatase (3.2 eV). Comparing the spectra

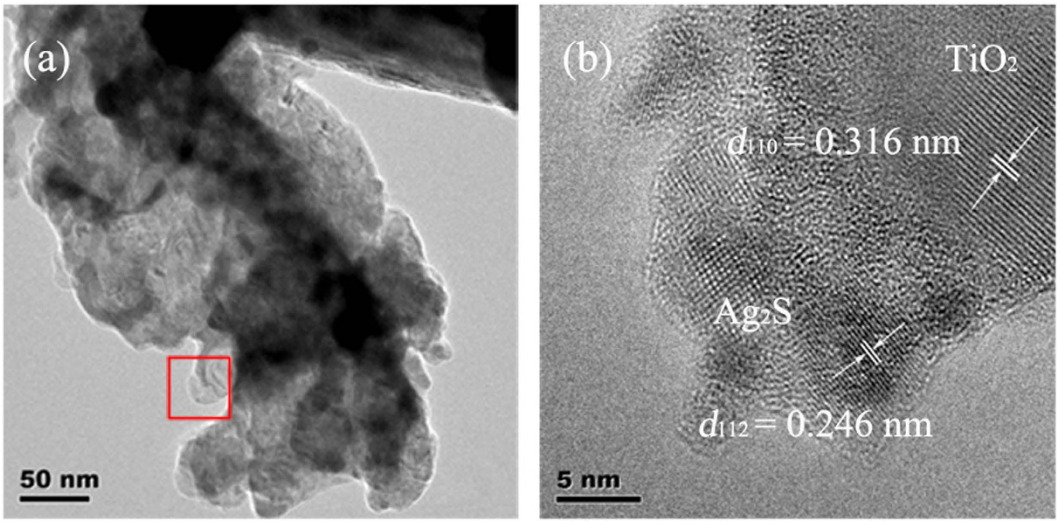

Figure 2. (**a**) TEM image and (**b**) the corresponding HRTEM image of Ag_2S-coupled TiO_2 NRAs by SILAR method for 35 cycles, corresponding to the rectangular region in (**a**).

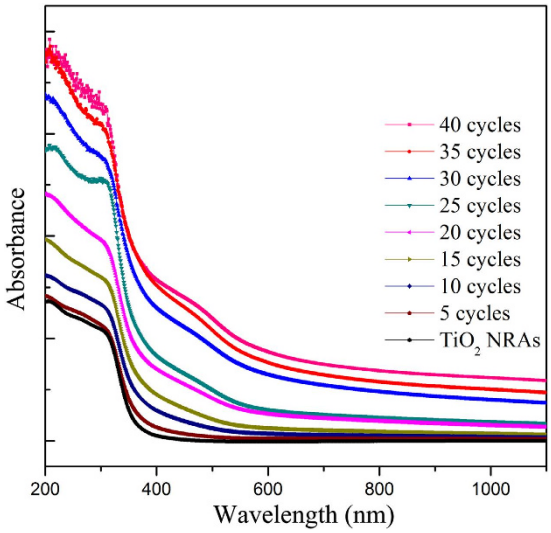

Figure 3. UV-visible absorption spectra of TiO_2 NRAs and Ag_2S-coupled TiO_2 for various cycles.

of the samples with different cycles, it can be seen that the absorption of Ag_2S-coupled TiO_2 NRAs displays an evident enhancement in the visible-light (~400–600 nm) region from 5 to 40 cycles. Meanwhile, the absorption of the samples shows red shifts with increasing cycles. This means the band gap of the samples has been reduced as increasing the amount of Ag_2S deposited on TiO_2 NRAs. With Ag_2S deposited on TiO_2 NRAs, the absorption spectra are successfully extended to visible light region. In addition, the evident gradual enhancement of absorption implies that the amount of Ag_2S increases with increasing depositing cycles. Therefore, compared with bare TiO_2, a better photochemical performance under visible light irradiation is expected in Ag_2S-coupled TiO_2 NRAs.

Visible-light-induced photoelectrochemical performance. To further investigate the electrochemical activity under visible light, *J-V* characteristics curves (Fig. 4) of the samples from 0 to 40 SILAR cycles were measured under dark condition and visible light (illuminated by a 300 W Xe lamp at 130 mW/cm^2, with UV light excluded by an ultraviolet cutoff filter), respectively. No significant photocurrent density was observed in the dark for all samples within the applied voltage range. While there were obvious photocurrent increases under visible-light illumination for all Ag_2S-coupled TiO_2 NRAs samples. It is also clear that compared with bare TiO_2 NRAs, Ag_2S-coupled TiO_2 NRAs samples show much higher photocurrent densities, indicating an enhanced separation and longer lifetime of photogenerated charge carriers. Moreover, it is noteworthy that with increasing cycles, the photocurrent densities increased from 5 cycles to 35 cycles, then decreased from 35 to 40 cycles, suggesting that there is an optimum amount of Ag_2S deposited on TiO_2 NRAs in terms of photoelectrochemical performance.

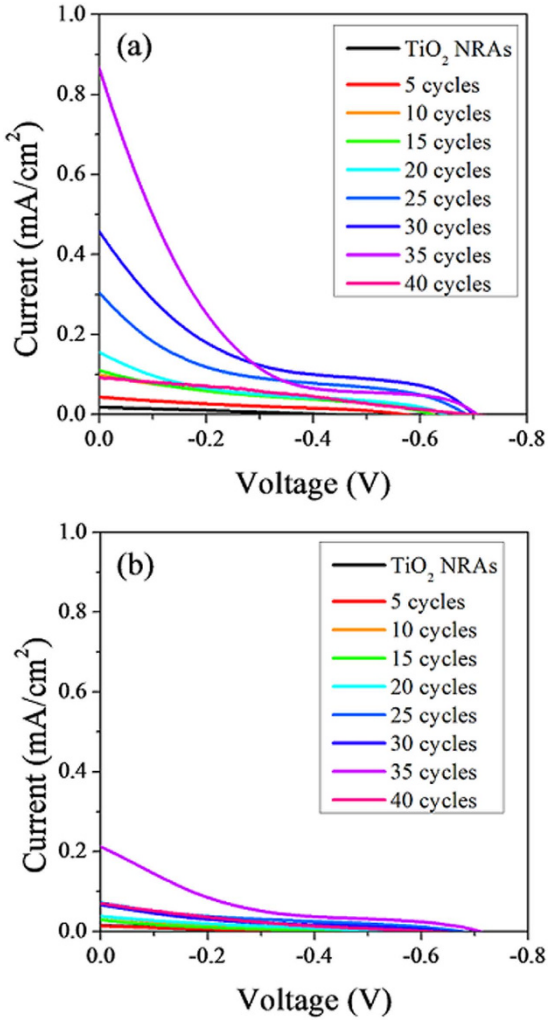

Figure 4. Photocurrent density-voltage curves of TiO_2 NRAs and Ag_2S-coupled TiO_2 for various cycles under (**a**) visible light irradiation and (**b**) dark condition.

Cycles	J_{sc} (mA/cm^2)	V_{oc} (V)	η (%)
0	0.062	0.420	0.002
5	1.227	0.568	0.006
10	1.343	0.623	0.017
15	1.112	0.620	0.015
20	1.547	0.645	0.017
25	2.844	0.687	0.034
30	4.243	0.699	0.046
35	6.256	0.707	0.054
40	0.302	0.692	0.019

Table 1. Parameters obtained from the photocurrent density-voltage curves of TiO_2 NRAs and Ag_2S-coupled TiO_2 for various cycles.

Based on the *J-V* characteristics curves, the photovoltaic properties parameters of these samples are listed in Table 1. From 0 (bare TiO_2 NRAs) to 35-cycle, all the electrochemical parameters increase at first, and then decrease from 35 to 40 cycles. This result is in accordance with the previous observation and confirms that with proper amount of Ag_2S NPs decorating TiO_2 NRAs the visible-light-induced photoelectrochemical activity is enhanced due to more effective separation of photogenerated electrons and holes. Overall, the electrochemical parameters reached a maximum value at 35 SILAR cycles. Further increase of Ag_2S leads to deterioration of performance, since an excess of Ag_2S NPs may destroy the one-dimensional structure of TiO_2 NRAs due to the aggregation around the nanorods, therefore impeding effective charge transportation. Similarly, a large amount

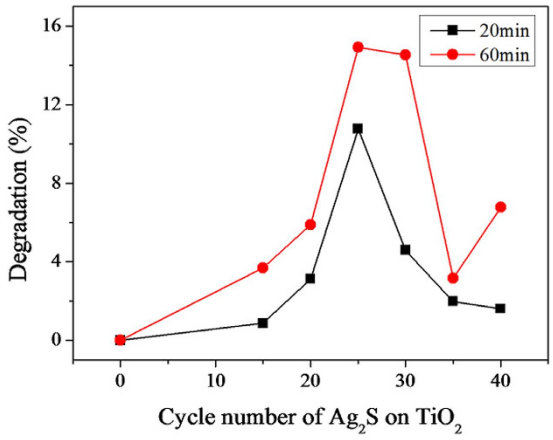

Figure 5. Photocatalytic degradation rates of MO under visible light irradiation using TiO_2 NRAs (0 cycle) and Ag_2S-coupled TiO_2 for various cycles for 20 min and 60 min, respectively.

of Ag_2S NPs may form more nanoclusters, which can become electron-hole recombination centers, causing unfavorable charge recombination and decreasing photoelectrochemical activity.

To evaluate the relative performance of samples with the optimized amount of Ag_2S, we can compare the results with bare TiO_2 NRAs. The 35-cycle-Ag_2S-coupled TiO_2 NRAs sample possesses the highest value of short circuit current density (J_{sc}), open circuit voltage (V_{oc}) and photovoltaic conversion efficiency (η), which is 6.256 mA/cm^2, 0.707 V and 0.054%, respectively. These electrochemical parameters reach 101, 1.68 and 26.5 times improvement more than bare TiO_2 NRAs, respectively. This suggests a pronounced enhancement of visible-light photoelectrochemical performance. Considering the length scale of nanomaterial, the 35-cycle sample shows promising absolute values of these properties.

Visible-light-induced photocatalytic performance. The photocatalytic activities of Ag_2S-coupled TiO_2 NRAs were explored by the degradation rate of methyl orange (MO) under visible light irradiation. Figure 5 shows the degradation percentage of MO solution degraded by bare TiO_2 (0 cycle) and Ag_2S/TiO_2 NRAs with various cycles under visible-light irradiation times of 20 and 60 min, respectively. In general, TiO_2 NRAs display a lower photodegradation rate of MO under visible-light irradiation. It is noteworthy that the degradation rate of MO obviously increases with the existence of certain amount of Ag_2S NPs on TiO_2 NRAs, and the 25-cycle sample reach the highest photocatalytic activity. This optimum photocatalytic performance shows around 3200-fold improvement in degradation rate compared with bare TiO_2 in the 60 min degradation process under visible-light irradiation. Photocatalytic activities of samples with various cycles increase before reaching the optimum amount then decrease to a lower level. This result is also in agreement with the conclusion of photoelectrochemical properties, which confirms the previous interpretation for the relationship between the amount of Ag_2S and photoelectrochemical performance. Electrochemical activity reaches optimum value at the 35-cycle sample, while photocatalytic activity reached the maximum value at the 25-cycle sample, indicating the performance of the photocatalyst in a real pollutant degradation reaction depends on multiple factors. Besides, the generation rate and lifetime of photogenerated charge carriers may be related to other factors such as surface area of the sample, particle size of the sensitizer, phase composition and reaction mechanism.

Conclusions

In summary, TiO_2 NRAs were prepared by the electron beam deposition with GLAD technique and successive annealing Ti NRAs. Using the SILAR method, we obtained Ag_2S-coupled TiO_2 NRAs, with various amounts of Ag_2S readily controlled by reaction cycle numbers.

By depositing Ag_2S on TiO_2 NRAs, the visible light response is notably enhanced in UV-visible absorption spectra. Photoelectrochemical and photocatalytic activity has also been remarkably improved under visible light irradiation and showed a significant variation with different reaction cycles. The 35-cycle Ag_2S-coupled TiO_2 NRAs reaches the maximum photocurrent density. The optimum photocatalytic rate appears on 25-cycle sample, which exhibits a notable visible-light-induced photocatalytic around 3200-fold improvement compared with bare TiO_2 NRAs in the 60 min MO degradation process. This method which can utilize visible light resources more efficiently provides a promising candidate for photocatalysis in the application of wastewater treatment and organic pollutant degradation.

To improve the photocatalytic performance of this binary system, prospective researches could be considered including modifying treatment such as ion irradiation[32], (rapid) thermal annealing[26,33], strong magnetic fields[34] and their synergy effect[35]. Moreover, promising techniques such as ion implantation[36] and light etching[37] induced patterning could be used to control the substrate for synthesizing NRAs. Also, apart from the SILAR method in this study, other surface deposition techniques (such as magnetron sputtering[38] and chemical vapor deposition[39]) could be applied to introduce Ag_2S NPs on TiO_2 NRAs.

Methods

Synthesis of TiO_2 NRAs. The TiO_2 NRAs were prepared by oxidation of Ti NRAs via annealing. The Ti NRAs were deposited by electron beam deposition using GLAD technique[40], on quartz, silicon wafer and F-doped SnO_2 (FTO) substrates, respectively. Quartz substrates were used for UV-vis transmittance measurement, silicon wafer for SEM observation and FTO for photo electrochemical measurement. The quartz, silicon wafer and FTO substrates were successively ultrasonically cleaned in acetone, alcohol and deionized water for 5 min each. With a base vacuum level of 2×10^{-8}Torr, Ti NRAs were deposited at a rate of 7.5 Å/s, where the thickness was monitored by a quartz crystal microbalance. To prepare vertically aligned Ti NRAs, the substrates rotated at a speed of 10 rpm while the incident beam of Ti flux was set at *ca.* 85° from the normal surface of the substrate. Then the Ti NRAs were annealed in a tube furnace under ambient atmosphere, from room temperature (~20 °C) to 450 °C in 90 minutes, maintained at 450 °C for 120 minutes, followed by furnace cooling to room temperature. Thus, the TiO_2 NRAs on these three different substrates were obtained.

Deposition of Ag_2S nanoparticles on TiO_2 NRAs. Ag_2S NPs were deposited on TiO_2 NRAs via SILAR method at room temperature. Briefly, the TiO_2 NRAs substrate was first immersed into a 0.05 M $AgNO_3$ aqueous solution for 30 s, next rinsed with deionized water, then immersed into a 0.05 M Na_2S aqueous solution for 30 s, and finally rinsed with deionized water again. This four-step procedure was considered as one SILAR cycle. The amount of Ag_2S NPs deposited could be accumulated by repeating the SILAR cycle. To obtain a series of samples with different amounts of Ag_2S NPs deposited on TiO_2 NRAs, this immersion cycle (n) was repeated different times in our work, specifically 5, 10, 15, 20, 25, 30, 35, 40 cycles.

Characterizations. The morphology of all the Ag_2S-coupled TiO_2 NRAs samples was characterized by a field emission scanning electron microscope (SEM JEOL-7001 F). The microstructures of the samples were also characterized with a transmission electron microscope (TEM JEOL-JEM2011). The UV-visible diffuse reflectance spectra (DRS) for the as-prepared samples were investigated using a UV-vis spectrophotometer (PerkinElmer Lambda 35).

Photoelectrochemical properties. Photoelectrochemical properties were investigated by measuring the photocurrent intensity versus potential (I-V curve) using an electrochemistry workstation (CHI 660d, Chenhua Instrument). These measurements were carried out in a 250 mL quartz cell using a standard three-electrode configuration, composed of the samples on FTO substrates as a working electrode, a Pt foil as a counter electrode, a saturated Ag/AgCl as a reference electrode, and 1 M Na_2S aqueous solution as the electrolyte. The working electrode was illuminated by a 300 W Xe lamp with power of ~130 mW/cm^2. An ultraviolet cutoff filter was inserted between the light source and the quartz cell to exclude UV light with a wavelength below 420 nm.

Photocatalytic properties. To evaluate the photocatalytic performance of samples, the photodegradation reactions of MO were performed. The decomposition of MO with the as-prepared Ag_2S-coupled TiO_2 NRAs was examined by its optical absorption spectroscopy. In typical photodegradation reactions, samples with uniformly-sized quartz substrates (15 mm × 15 mm) were added into 5.0 mL MO aqueous solution (1 mM) in a 10 mL beaker one at a time. Then, the system was placed in a petri dish filled with cooling water, and illuminated by the 300 W Xe lamp for 20 and 60 min, respectively, with a filter cutting off light with the wavelength below 420 nm. Before, during and after the reactions, a solution of 3.0 ml MO was drawn out to measure the concentration of MO using a UV-vis spectrophotometer (PerkinElmer Lambda 35). To differentiate the evaporation effect on the concentration of MO, a blank control system of 5.0 mL MO without photocatalytic samples was introduced during the degradation process.

References

1. Fujishima, A. & Honda, K. Photolysis-decomposition of water at the surface of an irradiated semiconductor. *Nature* **238,** 37–38 (1972).
2. Asahi, R., Morikawa, T., Ohwaki, T., Aoki, K. & Taga, Y. Visible-light photocatalysis in nitrogen-doped titanium oxides. *Science* **293,** 269–271 (2001).
3. Li, Z. C., Zhu, Y., Zhou, Q., Ni, J. & Zhang, Z. J. Photocatalytic properties of TiO_2 thin films obtained by glancing angle deposition. *Appl. Surf. Sci.* **258,** 2766–2770 (2012).
4. Linsebigler, A. L., Lu, G. & Yates, J. T. Photocatalysis on TiO_2 surfaces: principles, mechanisms, and selected results. *Chem. Rev.* **95,** 735–758 (1995).
5. Li, Z. C., Xing, L. P., Zhang, N., Yang, Y. & Zhang, Z. J. Preparation and photocatalytic property of TiO_2 columnar nanostructure films. *Mater. Trans.* **52,** 1939–1942 (2011).
6. Wang, J. W., Mao, B. D., Gole, J. L. & Burda, C. Visible-light-driven reversible and switchable hydrophobic to hydrophilic nitrogen-doped titania surfaces: correlation with photocatalysis. *Nanoscale* **2,** 2257–2261 (2010).
7. Li, Z. C., Teng, Y., Xing, L. P., Zhang, N. & Zhang, Z. J. Enhancement of the photocatalytic property of TiO_2 columnar nanostructured films by changing deposition angle. *Mater. Res. Bull.* **50,** 68–72 (2014).
8. Romero, M. *et al.* Solar photocatalytic degradation of water and air pollutants: challenges and perspectives. *Sol. Energy* **66,** 169–182 (1999).
9. Zhu, K., Neale, N. R., Miedaner, A. & Frank, A. J. Enhanced charge-collection efficiencies and light scattering in dye-sensitized solar cells using oriented TiO_2 nanotubes arrays. *Nano Lett.* **7,** 69–74 (2007).
10. Mor, G. K., Shankar, K., Paulose, M., Varghese, O. K. & Grimes, C. A. Use of highly-ordered TiO_2 nanotube arrays in dye-sensitized solar cells. *Nano Lett.* **6,** 215–218 (2006).
11. Anpo, M. & Takeuchi, M. The design and development of highly reactive titanium oxide photocatalysts operating under visible light irradiation. *J. Catal.* **216,** 505–516 (2003).
12. Yamashita, H., Honda, M., Harada, M., Ichihashi, Y. & Anpo, M. Preparation of titanium oxide photocatalysts anchored on porous silica glass by a metal ion-implantation method and their photocatalytic reactivities for the degradation of 2-propanol diluted in water. *J. Phys. Chem. B* **102,** 10707–10711 (1998).
13. Rengifo-Herrera, J. A. *et al.* Synthesis, characterization, and photocatalytic activities of nanoparticulate N, S-codoped TiO_2 having different surface-to-volume ratios. *J. Phys. Chem. C* **114,** 2717–2723 (2010).

14. Kang, M. G., Han, H. E. & Kim, K. J. Enhanced photodecomposition of 4-chlorophenol in aqueous solution by deposition of CdS on TiO_2. *J. Photochem. Photobiol. A-Chem.* **125,** 119–125 (1999).
15. Gao, B., Kim, Y. J., Chakraborty, A. K. & Lee, W. I. Efficient decomposition of organic compounds with $FeTiO_3/TiO_2$ heterojunction under visible light irradiation. *Appl. Catal. B: Environ.* **83,** 202–207 (2008).
16. Wang, M. *et al.* C. J. p-n Heterojunction photoelectrodes composed of Cu_2O-loaded TiO_2 nanotube arrays with enhanced photoelectrochemical and photoelectrocatalytic activities. *Energy Environ. Sci.* **6,** 1211–1220 (2013).
17. Zhou, W. J. *et al.* Ag_2O/TiO_2 nanobelts heterostructure with enhanced ultraviolet and visible photocatalytic activity. *ACS Appl. Mater. Interfaces* **2,** 2385–2392 (2010).
18. Xie, Z. *et al.* Enhanced photoelectrochemical properties of TiO_2 nanorod arrays decorated with CdS nanoparticles. *Sci. Technol. Adv. Mater.* **15,** 055006 (2014).
19. Kumar, S. G. & Devi, L. G. Review on modified TiO_2 photocatalysis under UV/visible light: selected results and related mechanisms on interfacial charge carrier transfer dynamics. *J. Phys. Chem. A* **115,** 13211–13241 (2011).
20. Han, F., Kambala, V. S. R., Srinivasan, M., Rajarathnam, D. & Naidu, R. Tailored titanium dioxide photocatalysts for the degradation of organic dyes in wastewater treatment: a review. *Appl. Catal. A-Gen.* **359,** 25–40 (2009).
21. Besselchouad, Y. *et al.* UV–vis versus visible degradation of Acid Orange II in a coupled CdS/TiO_2 semiconductors suspension. J. *Photochem. Photobiol. A: Chem.* **183,** 218–224 (2006).
22. Tada, H., Fujishima, M. & Kobayashi, H. Photodeposition of metal sulfide quantum dots on titanium (IV) dioxide and the applications to solar energy conversion. *Chem. Soc. Rev.* **40,** 4232–4243 (2011).
23. Levine, L. H., Coutts, J. L., Richards, J. T., Hintze, P. E. & Clausen, C. A. Review on transforming TiO_2 into a visible-light-responsive catalyst for water and air purification. 42nd International Conference on Environmental Systems. (San Diego: California, 2012).
24. Galléa, F., Li, Z. C. & Zhang, Z. J. Growth control of tungsten oxide nanostructures on planar silicon substrates. *Appl. Phys. Lett.* **89,** 193111 (2006).
25. Xie, Y., Heo, S. H., Kim, Y. N., Yoo, S. H. & Cho, S. O. Synthesis and visible-light-induced catalytic activity of Ag_2S-coupled TiO_2 nanoparticles and nanowires. *Nanotechnology* **21,** 015703 (2010).
26. Wei, Q., Zhang, Z. J., Li, Z. C., Zhou, Q. & Zhu, Y. Enhanced photocatalytic activity of porous α-Fe_2O_3 films prepared by rapid thermal oxidation. *J. Phys. D-Appl. Phys.* **41,** 202002 (2008).
27. Shen, H. P., Jiao, X. J., Oron, D., Li, J. B. & Lin, H. Efficient electron injection in non-toxic silver sulfide (Ag_2S) sensitized solar cells. *J. Power Sources* **240,** 8–13 (2013).
28. Shaislamov, U. & Yang, B. L. CdS-sensitized single-crystalline TiO_2 nanorods and polycrystalline nanotubes for solar hydrogen generation. *J. Mater. Res.* **28,** 418–23 (2013).
29. Gholami, M., Qorbani, M., Moradlou, O., Naseri, N. & Moshfegh, A. Z. Optimal Ag_2S nanoparticle incorporated TiO_2 nanotube array for visible water splitting. *RSC Adv.* **4,** 7838–7844 (2014).
30. Hu, H. W. *et al.* Photodeposition of Ag_2S on TiO_2 nanorod arrays for quantum dot-sensitized solar cells. *Nanoscale Res. Lett.* **8,** 1–7 (2013).
31. Liu, B. K. *et al.* Photoelectrical properties of Ag_2S quantum dot-modified TiO_2 nanorod arrays and their application for photovoltaic devices. *Dalton Trans* **42,** 2232–2237 (2013).
32. Li, Z. C. *et al.* Effect of Xe ion irradiation on photocatalytic performance of oblique TiO_2 nanowire arrays. *Appl. Surf. Sci.* **327,** 478–482 (2015).
33. Liu, J. *et al.* Temperature annealing of tracks induced by ion irradiation of graphite. *Nucl. Instrum. Methods Phys. Res. Sect. B-Beam Interact. Mater. Atoms* **245,** 126–129 (2006).
34. Hu, Y., Li, Z. C., Zhang, Z. J. & Meng, D. Q. Effect of magnetic field on the visible light emission of V_2O_5 nanorods, *Appl. Phys. Lett.* **94,** 103107 (2009).
35. Zhan, P., Wang, W. P., Xie, Q., Li, Z. C. & Zhang, Z. J. Enhanced room-temperature ferromagnetism in un-doped ZnO thin films by thermal annealing in a strong magnetic field. *J. Appl. Phys.* **111,** 103524 (2012).
36. Hu, Y., Li, Z. C. & Zhang, Z. J. Ion-implantation-induced patterns formation on silicon substrates. *Physica E*, **41,** 833–837 (2009).
37. Zhang, X., Zhou, Q., Ni, J., Li, Z. C. & Zhang, Z. J. Surface-enhanced Raman scattering from a hexagonal lattice of micro-patterns of vertically aligned Ag nanorods. *Physica E* **44,** 460–463 (2011).
38. Lv, S. S., Li, Z. C., Liao, J. C., Zhang, Z. J. & Miao, W. Well-aligned NiSi/Si heterostructured nanowire arrays as field emitters. *J. Vac. Sci. Technol. B* **33,** 02B101 (2015).
39. Lee, J. C., Kim, T. G., Lee, W., Han, S. H. & Sung, Y. M. Growth of CdS Nanorod-Coated TiO_2 Nanowires on Conductive Glass for Photovoltaic Applications. *Cryst. Growth Des.* **9,** 4519–4523 (2009).
40. Zhou, Q., Li, Z. C., Ni, J. & Zhang, Z. J. A simple model to describe the rule of glancing angle deposition. *Mater. Trans.* **52,** 469–473 (2011).

Acknowledgements

The authors are grateful to the financial support by the National Natural Science Foundation of China (under Grant 61176003).

Author Contributions

S.X. and Z.L. designed the study, proposed the mechanism, and wrote the manuscript. S.X., Z.X. and G.W. performed the experiments and analyzed the data. Z.Z. gave many suggestions during this work process. All authors reviewed the manuscript.

Additional Information

Competing financial interests: The authors declare no competing financial interests.

How to cite this article: Li, Z. *et al.* Role of Ag_2S coupling on enhancing the visible-light-induced catalytic property of TiO_2 nanorod arrays. *Sci. Rep.* **6**, 19754; doi: 10.1038/srep19754 (2016).